J Appl Electrochem (2007) 37:605–616
DOI 10.1007/s10800-007-9291-7

ORIGINAL PAPER

Adaptive, multi-parameter battery state estimator with optimized time-weighting factors

Mark Verbrugge

Received: 15 May 2006 / Accepted: 3 January 2007 / Published online: 21 February 2007

Abstract We derive and implement a battery control algorithm that can accommodate an arbitrary number of model parameters, with each model parameter having its own time-weighting factor, and we propose a method to determine optimal values for the time-weighting factors. Time-weighting factors are employed to give greater impact to recent data for the determination of a system's state. We employ the (controls) methodology of weighted recursive least squares, and the time weighting corresponds to the exponential-forgetting formalism. The output from the adaptive algorithm is the battery state of charge (remaining energy), state of health (relative to the battery's nominal performance), and predicted power capability. Results are presented for a high-power lithium ion battery.

Keywords Battery · Control · Equivalent circuit · Mathematical model · Power prediction · State of charge prediction · Weighted recursive least squares

List of symbols

Ah	Coulombic capacity, C-h/s
A	$1/C_D$, 1/F
b	Regressed intercept
B	$1/ (R_{ct}\ C_D)$, 1/s
C_D	Capacitance, F
I	Current, A
L	Number of parameters m to be regressed adaptively
m	Parameter to be regressed
N	Number of time steps (data points) in the regression
P	Power, W
r	Capacitance ratio, $C_{D,\text{discharge}}/C_{D,\text{charge}}$
R	High-frequency resistance, ohm
R_{ct}	Effective interfacial resistance, ohm
SOC	Percent state of charge (energy content in the battery relative to the energy content upon full charge)
SOH	State of health, Eq. 15
s	Sum
t	Time, s
V	System voltage, V
V_H	Hysteresis voltage, V
V_{oc}	Open-circuit voltage, V
x	Time-dependent values multiplying onto parameters m
y	Dependent variable
w_{SOC}	Weighting factor (Eq. 17)
β	Hysteresis parameter, C^{-1}
ε	Error or loss term
$\boldsymbol{\varepsilon}_{opt}$	Unweighted total error as defined by Eq. 13
λ	Forgetting factor (Eq. 2)
γ	Parameter for selective weighting of data beyond that of the forgetting factor
η_I	Current efficiency
σ	Variance

M. Verbrugge (✉)
General Motors Research and Development, Mailcode 480-106-224, 30500 Mound Rd., P.O. Box 9055, Warren, MI 48090-9055, USA
e-mail: mark.w.verbrugge@gm.com

1 Introduction

For efficient energy management of a system employing batteries or supercapacitors, an adaptive algorithm that

can characterize the state of the energy-storage device is required. Inputs to the algorithm include the system current, voltage, and temperature, and outputs characterize the energy content (state of charge, or SOC), predicted power capability (state of power, or SOP), and performance relative to the new and end-of-life condition (state of health, or SOH). For automotive applications, the conversion of input information to outputs must be fast and not require substantial amounts of computer storage, consistent with embedded-controller and serial-data-transfer capabilities. Generally these two limitations mandate that algorithms be fully recursive, wherein all information utilized by the algorithm stems from previous time-step values and measurements that are immediately available.

To construct a state estimator for the SOC, SOH, and SOP, model reference adaptive systems [1–5] can be employed. For this approach, a model of the plant (e.g., the battery) is constructed, and the parameters appearing in the model are regressed from the available measurements. For example, using the equivalent circuit depicted in Fig. 1, one can construct a mathematical expression for a battery, and the values of the circuit elements can be regressed from the available current, voltage, and temperature data during vehicle operation. The method of weighted recursive least squares (WRLS) with exponential forgetting has proven to be a pragmatic approach for parameter regression [6–14] when model reference adaptive systems are employed. The time weighting of data is damped exponentially with this approach; hence, new data has a preferential impact in determining the value of regressed parameters and thus the state of the system.

Two issues arise in the standard implementation of WRLS. First, one would like to assign a time-weighting factor for each of the parameters extracted instead of single forgetting factor as is commonly employed [3–14]; this is an active area of research within the controls community [15–21]. It will be shown in this work that a substantially more accurate state estimator for SOC, SOH, and SOP is obtained when individual forgetting factors are incorporated. Second, it is desirable to select the value of the forgetting factors using an optimization function. In this paper we (1) propose a method based on WRLS such that forgetting factors can be assigned to each individual parameter to be regressed and (2) provide a means to determine the optimal values of the forgetting factors. The approach is applied to a high-power-density lithium ion battery.

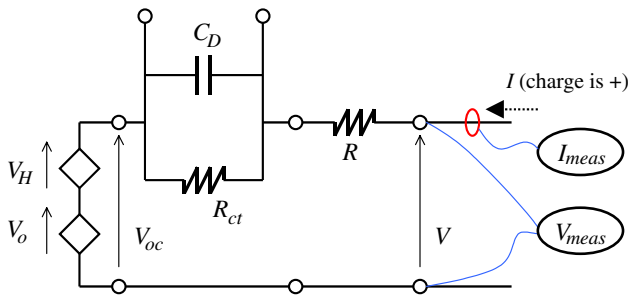

Fig. 1 Equivalent circuit used as the model of the battery system. Positive currents denote the battery charging process

2 Parameter regression method

We begin with the instantaneous error ε (often referred to as the loss term),

$$\varepsilon(t) = [y - (m_1x_1 + m_2x_2 + \ldots + m_Lx_L + b)], \tag{1}$$

where y represents the experimentally obtained dependent variable at time t (i.e., $y = V^{\text{measured}}$, the measured voltage for the energy storage system) and the values x_1, x_2, ..., x_L represent the measured quantities on which the L parameters m_1, m_2, ..., m_L multiply, respectively, to complete the linear model once the parameter b [resulting from the regressed open-circuit potential in the case of energy storage devices (2, 4, 5)] is included. We shall not address nonlinear models in this communication. Because we shall formulate an iterative scheme that does not require matrix inversion, it is expedient to fold b into the parameter vector $\mathbf{m} = [m_1,m_2,\ldots,m_L]^T$, recognizing that the corresponding value of x associated with b is unity, as will be made clear below (Eq. 12). The weighted square of the error term summed over N data points can be expressed as

$$\varepsilon_l = \sum_{j=1,N} \gamma_j \lambda^{N-j} \left[y_j - (m_1x_{1,j} + m_2x_{2,j} + \ldots + m_{L,j}x_{L,j})\right]^2. \tag{2}$$

For a system wherein only one of the L parameters changes with time, designated as m_l, and all others correspond to fixed values, the weighted square of the error associated with the single parameter l is

$$\varepsilon_l = \sum_{j=1,N} \gamma_{l,j} \lambda_l^{N-j} \left[y_j - m_l x_{l,j} - \sum_{k=1,\neq l}^{k=L} m_k x_{k,j} \right]^2. \tag{3}$$

Two clarifications must be provided for Eqs. 2 and 3. First, there are instances when some data should be given more or less weighting on a basis other than time. For example, the equivalent circuit model we employ

to correlate battery behavior does not address gassing reactions on charge [22], and we may choose to give a larger weighting to discharge data relative to charge data. For this reason, the composite weight factor corresponds to $\gamma\ \lambda$, with the factor γ provided so as to weight selectively various data, while λ corresponds to the standard exponential forgetting factor for time-weighting data [5–14]; larger (composite) weight factors give rise to larger impacts on the error ε and thus more influence with regard to evaluating the parameters m_l. Second, recall that all of the L parameters may vary with time. Our approach is to let only one parameter (denoted by subscript l) change relative to its previously calculated value, and the remaining L–1 parameters are fixed at their values obtained from the previous time step (i.e., at their regressed values corresponding to time t–Δt and the integer time index $j = N - 1$). Thus Eq. 3 specifies that the exponential forgetting factor λ (and the factor γ) is to be associated with a parameter l; up to this point our formulation is similar to that of Vahidi et al. (cf. Eq. 13 of Reference [20]).

Consistent with Eqs. 2 and 3, we shall term the total error as the square of the sum of the L individual errors,

$$\varepsilon = \sum_{l=1,L} \varepsilon_l = \sum_{l=1,L} \sum_{j=1,N} \gamma_{l,j} \lambda_l^{N-j} \left[y_j(t) - m_l(t) x_{l,j}(t) - \sum_{k=1,L,\ k \neq l} m_k(t-\Delta t) x_{k,j}(t) \right]^2 . \tag{4}$$

By minimizing the total error ε with respect to m_l at time step N [employing Eq. 4 to determine $\partial\varepsilon/\partial m_l(t) = 0$], we obtain an equation for the l'th parameter m_l:

$$m_{l,N} = \frac{1}{\sum_{j=1,N} \gamma_{l,j} \lambda_l^{N-j} x_{l,j}^2} \left(\sum_{j=1,N} \gamma_{l,j} \lambda_l^{N-j} y_j x_{l,j} - \sum_{k=1,L,\ k \neq l} m_{k,N-1} \sum_{j=1,N} \gamma_{l,j} \lambda_l^{N-j} x_{k,j} x_{l,j} \right) . \tag{5}$$

One can view this approach as the sequential minimization of the total error term with respect to individual parameters. This relation can be used to regress individually each of the L parameters at time step N, and we now have an expression reflecting a weight factor λ_l for each of the L parameters m_l. Equation 5 is implemented L times at each time step, with the l ranging from 1 to L. Thus there are no matrix equations to solve in this approach, and the method can be viewed as iterative. We do not address parameter convergence [16], which remains an open question.

For illustrative purposes, it is helpful to view a two parameter model,

$$y = m_1 x_1 + m_2 x_2 . \tag{6}$$

For a battery system, this could correspond to an ''ohmic battery,'' wherein the hysteresis and parallel resistor-capacitor contributions to the equivalent circuit in Figure 1 are removed:

$$\begin{aligned} V &= V_{oc} + IR \\ y &= V^{\text{measured}} \\ m_1 &= V_{oc} \\ m_2 &= R \\ x_1 &= 1 \\ x_2 &= I \end{aligned} , \tag{7}$$

and $V = V_{oc} + IR = m_1 x_1 + m_2 x_2$. The total error is written as

$$\begin{aligned} \varepsilon = \sum_{j=1}^{N} & \gamma_{1,j} \lambda_1^{N-j} \left[y_j(t) - m_1(t) x_{1,j}(t) - m_2(t-\Delta t) x_{2,j}(t) \right]^2 \\ & + \gamma_{2,j} \lambda_2^{N-j} \left[y_j(t) - m_2(t) x_{2,j}(t) - m_1(t-\Delta t) x_{1,j}(t) \right]^2 \end{aligned} . \tag{8}$$

The parameters (R and V_{oc}) can be regressed using the following

$$\begin{aligned} m_{1,N} = & \frac{1}{\sum_{j=1,N} \gamma_{1,j} \lambda_1^{N-j} x_{1,j}^2} \\ & \times \sum_{j=1,N} \left[\gamma_{1,j} \lambda_1^{N-j} y_j x_{1,j} - m_{2,N-1} \gamma_{1,j} \lambda_1^{N-j} x_{2,j} x_{1,j} \right] \\ m_{2,N} = & \frac{1}{\sum_{j=1,N} \gamma_{2,j} \lambda_2^{N-j} x_{2,j}^2} \\ & \times \sum_{j=1,N} \left[\gamma_{2,j} \lambda_2^{N-j} y_j x_{2,j} - m_{1,N-1} \gamma_{2,j} \lambda_2^{N-j} x_{1,j} x_{2,j} \right] \end{aligned} , \tag{9}$$

with λ_1 and λ_2 being the forgetting factors for m_1 and m_2, respectively.

For the general case of L parameters, we can make Eq. 5 fully recursive with the following definitions:

$$\begin{aligned} s_{x,l}|_N &= \sum_{j=1,N} \gamma_{l,j}\lambda_l^{N-j}x_{l,j}^2 = \gamma_{l,N}x_{l,N}^2 + \lambda_l(s_{x,l}|_{N-1}) \\ s_{yx,l}|_N &= \sum_{j=1,N} \gamma_{l,j}\lambda_l^{N-j}y_j x_{l,j} = \gamma_{l,N}y_N x_{l,N} + \lambda_l(s_{yx,l}|_{N-1}) \\ s_{xx,l}|_N &= \sum_{j=1,N} \gamma_{l,j}\lambda_l^{N-j}x_{k,j}x_{l,j} = \gamma_{l,N}x_{k,N}x_{l,N} + \lambda_l(s_{xx,l}|_{N-1}) \end{aligned} \tag{10}$$

These recursive expressions can be used to recast Eq. 5 as

$$m_{l,N} = \frac{1}{s_{x,l}|_N}\left[s_{yx,l}|_N - \sum_{\substack{k=1,L \\ k\neq l}} m_{k,N-1}(s_{xx,l}|_N) \right]. \tag{11}$$

This expression is used for each of the L parameters m_l at each time step. As noted previously, no matrix inversion is required.

For the equivalent circuit employed to represent the battery system (Fig. 1), the following assignments can be made for the voltage expression (cf. Eq. 26 of the Appendix):

$$\begin{aligned} y &= V^{\text{measured}}|_t \\ x_1 &= I_t \\ x_2 &= (V^{\text{measured}} - V_{oc} - IR)_{t-\Delta t} \\ x_3 &= \left(\tfrac{I_{t-\Delta t}+I_t}{2}\right)\left[r_{(I_t+I_{t-\Delta t})/2}\right]\Delta t \\ x_4 &= w_H \Delta t\left\{(\eta_1 I - S_D)[V_{H,\max} - \text{sign}(I)V_H]\right\}_{t-\Delta t} \\ x_5 &= 1 \\ m_1 &= R \\ m_2 &= \exp(-B\Delta t) = e^{-\Delta t/\tau} = E \\ m_3 &= A_d \\ m_4 &= \beta \\ m_5 &= V_o + (V_H)_{t-\Delta t} \end{aligned} \tag{12}$$

3 Experimental

The lithium ion battery we investigate was developed by SAFT and is representative of the new generation of lithium ion batteries for hybrid vehicle use. Energy content is relatively low for this cell in order to minimize mass for high-power applications, and the specific power is very high; the power performance is comparable to that of activated carbon (nonaqueous solvent) supercapacitors. We employ the data reported in Reference [5] for this analysis; the independently measured parameter values at room temperature are provided in Table 1. The precise form of the power versus time trace is not important for the purposes of this work. Rather, it is helpful to generate a power versus time trace reflecting the intended application so as to examine the viability of the proposed algorithm. Hence the synthetic cycle discussed in Reference [5] is employed, and we outline some of the essential boundary conditions and experimental conditions in the remainder of this section.

Table 1 Cell parameters. The ratio r is fixed, and the uppermost five rows correspond to nominal values (independently measured) for the adapted parameters in the weighted recursive least squares (WRLS) algorithm [5]. The middle five rows ($C_{D,dis}$ to R) correspond to electrochemical parameters of interest that are extracted from the above parameters. For all plots shown in this work, the charge current efficiencies were taken to be unity, *Skew_cal* = 10 and γ = 1

Value	Quantity, units
1.637	R, mohm
0.905	E
8.000×10^{-5}	A_d, 1/F
1.122×10^{-4}	β, 1/C
3.9	V_o, V
0.75	$r = C_{D,dis}/C_{D,chg}$
12500	$C_{D,dis}$, F
16667	$C_{D,chg}$, F
5.00	τ, s
0.4	$R_{ct,dis}$, mohm
0.3	$R_{ct,chg}$, mohm
20	$V_{H,max}$, mV
4.2	*Ah*

Testing of the cell was conducted with a MACCOR Series 4000 battery cycler. Voltage was measured at the cell terminals with accuracy of ± 1 mV and resolution of 0.08 mV, and current was measured with accuracy of ±0.8 A and resolution of 0.01 A. At all times the cell was constrained to a voltage maximum of 3.9 V and a voltage minimum of 2.5 V. In cases where the voltage limit was met, the current magnitude was reduced such that the cell voltage was maintained at the limit for the remainder of the pulse. A maximum charge current limit of 120 A was also enforced. Cell temperature was measured by a thermocouple placed on the exterior surface of the cell can with ± 0.5 °C accuracy and 0.1 °C resolution. The required ambient temperature was maintained throughout each test by a Thermotron S4-C thermal chamber. The cell was placed in the chamber such that it was exposed to airflow on all sides.

4 Results

The open-circuit potential V_o for the lithium ion battery is shown in Fig. 2. We have bounded the

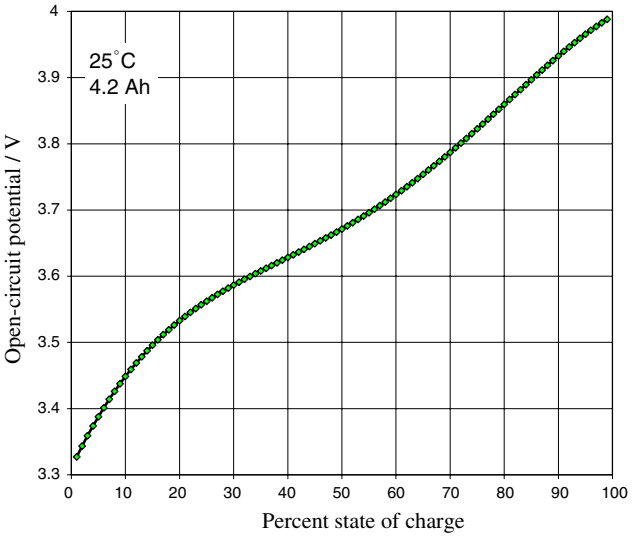

Fig. 2 Open circuit potential V_o. Potentials above 4 V and below 3.3 V are treated as 100% SOC and 0% SOC, respectively

values of parameters to be regressed as follows. The hysteresis parameter β was bounded between 0.5 and 2 times the nominal value listed in Table 1. The high-frequency resistance R was allowed to vary between 0.05 and 20 times the nominal value listed in Table 1, and the parameter E was allowed to vary between 0.5 and 0.95. Last, the parameter A_d was allowed to vary between 0.8 and 3 times the nominal value listed in Table 1. We do not have a specific procedure to propose for determining appropriate parameters bounds, and this remains an important open question.

The state of charge and measured (V), equilibrium (V_o) and hysteresis (V_H) voltages are shown in Fig. 3 for a fixed forgetting factor. Discharge of the battery at the completion of the indicated experiment yielded a capacity that was within ± 2.5 percent of the final SOC (about 50% at the end of the experiment depicted in Fig. 3). For the case of fixed and variable forgetting factors, the error for the entire data set (10,000 seconds in the case of Fig. 3, with the time per data point being 0.5 s and N = 20,000) was minimized to find the optimal values. We define the unweighted total error to be minimized as:

$$\begin{aligned}\varepsilon_{opt} &= \sum_{j=1,N}\left[V_j^{\text{measured}} - V_j^{\text{model}}\right]^2 \\ &= \sum_{j=1,N}\left[V_j^{\text{measured}} - \sum_{k=1,L} m_{k,j}x_{k,j}\right]^2\end{aligned} \tag{13}$$

Newton's method [23] was employed to optimize the forgetting factors:

$$\boldsymbol{\lambda}^{(n+1)} = \boldsymbol{\lambda}^{(n)} - \frac{\varepsilon_{opt}{}^{(n)}}{\varepsilon'_{opt}{}^{(n)}}, \tag{14}$$

where $\boldsymbol{\varepsilon}'_{opt}(\boldsymbol{\lambda})$ is the Jacobian matrix of the unweighted total error term that we minimize by determining the optimal values of the forgetting factor vector $\boldsymbol{\lambda}$ for the entire data set; the superscript (n) refers to the step in the Newton iteration. For this work, we found convergence ($\lambda_l^{(n+1)}/\lambda_l^{(n)} < 10^{-6}$) was obtained in about six iterations. For a fixed forgetting factor (Fig. 3, upper plot), the optimal value of λ is 0.9847. (For the case of a constant forgetting factor, $\boldsymbol{\lambda} = \lambda$, a single-valued scalar quantity.) The optimal values for the individual forgetting factors employed in the lower plot were close to values shown in the inset table of Fig. 6, which is discussed below. It is notable that the equilibrium potential V_o in the lower curves shows more oscillation with time and follows the variation in the current source. In experimenting with the variable forgetting factors, we learned that while a larger forgetting factor is appropriate for some parameters, the forgetting factor for V_o must be smaller in order to capture SOC variations with current.

Hybrid electric vehicles with relatively small batteries relative to the energy content of the on-board fuel (e.g., gasoline) tank are run in a charge-sustaining mode, versus a vehicle that can charge off the electrical grid, often termed a ''plug-in'' hybrid. Charge-sustaining hybrids are more common, as the costs of the battery as well as that of the electric motors and power electronics are reduced relative to plug-in hybrids. To maintain charge-sustaining operation, the battery is cycled about a set point SOC, generally near 50% SOC; we shall restrict much of our analysis to this condition. Analogous to the lower plot in Fig. 3, the state of charge and measured (V), equilibrium (V_o) and hysteresis (V_H) voltages are depicted in Fig. 4; the algorithm was started at 4,500 s (cf. Fig. 3), facilitating the analysis of algorithm operation about 50% SOC. The forgetting factors were optimized (Eq. 4) as will be discussed further in the context of Fig. 5. Only the results for the case of variable forgetting factors are shown in Fig. 4, as the results for the analogous (optimized) fixed forgetting factor was similar in appearance as plotted.

To appreciate the influence of the forgetting factor on the unweighted total error ε_{opt} (Eq. 13), we turn to Fig. 5. The ordinate values correspond to the unweighted total error ε_{opt} normalized by that which is obtained for the optimal fixed forgetting factor (0.9847 for the upper plot and 0.9827 for the lower plot). The upper plot corresponds to the analyses of Fig. 3, and

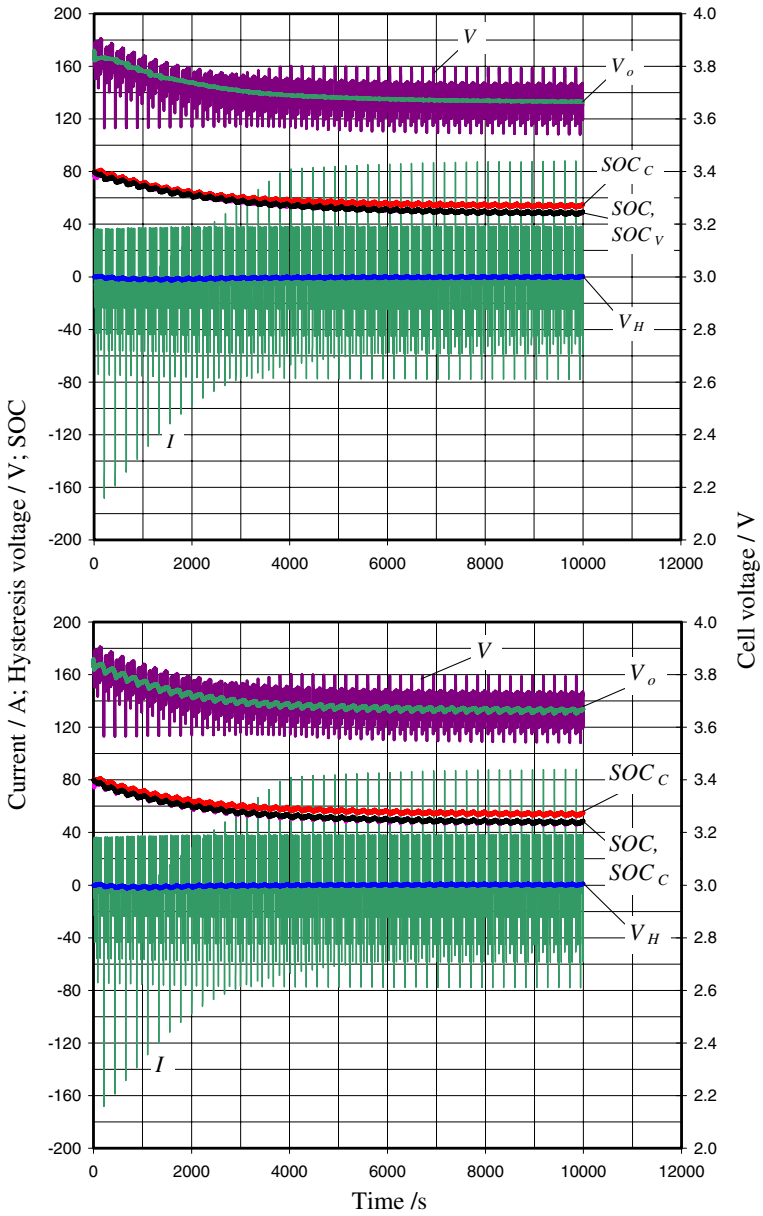

Fig. 3 State of charge, current (I), and measured (V), equilibrium (V_o) and hysteresis (V_H) voltages. Upper plot: fixed, optimized forgetting factor of 0.9847. Lower plot: optimized, variable forgetting factors. The quantities I and V are measured and the other values are regressed

the lower plot to those of Fig. 4. The unweighted total error is increased by 18% (top) and 53% (bottom) in going from variable forgetting factors to a fixed forgetting factor. Hence, employing a variable forgetting factor for a charge-sustaining hybrid utilizing a lithium ion battery can be expected to increase the accuracy of the algorithm by about 50%. In support of the optimal fixed forgetting factors of 0.9847 and 0.9827 depicted in Fig. 5, a single (fixed) value of 0.99 was used in References [4] and [5] for lead acid, NiMH, and lithium ion cells after the authors had gained some familiarity and experience with the algorithm. The optimization process employed in this work provides a quantitative basis for why a value near 0.99 worked well for the case of fixed forgetting factors. That is, while 0.99 was chosen without any quantitative insight in References [4] and [5], we find here the total error is minimized with a constant forgetting factor quite close to 0.99 (0.9847 and 0.9827 depicted in Fig. 5).

The optimized values for the variable forgetting factors and the associated parameter values m_l are shown in Fig. 6 for the analysis shown in Fig. 4. Four of the extracted parameters are displayed in the lower plot, and the fifth (V_o) is shown in Fig. 4. The lower plot in Fig. 6 shows that the parameters effectively converge within about 50 s (see the R and E curves, in particular). The high-frequency resistance R is seen to be quite stable, and a large forgetting factor, reflecting

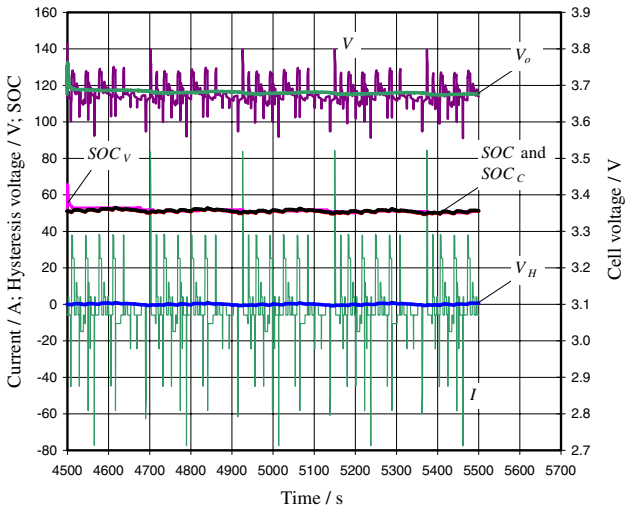

Fig. 4 State of charge and measured (V), equilibrium (V_o) and hysteresis (V_H) voltages. The algorithm was started at 4,500 s (cf. Fig. 3), facilitating the analysis of algorithm operation about charge-sustaining operation near 50% SOC

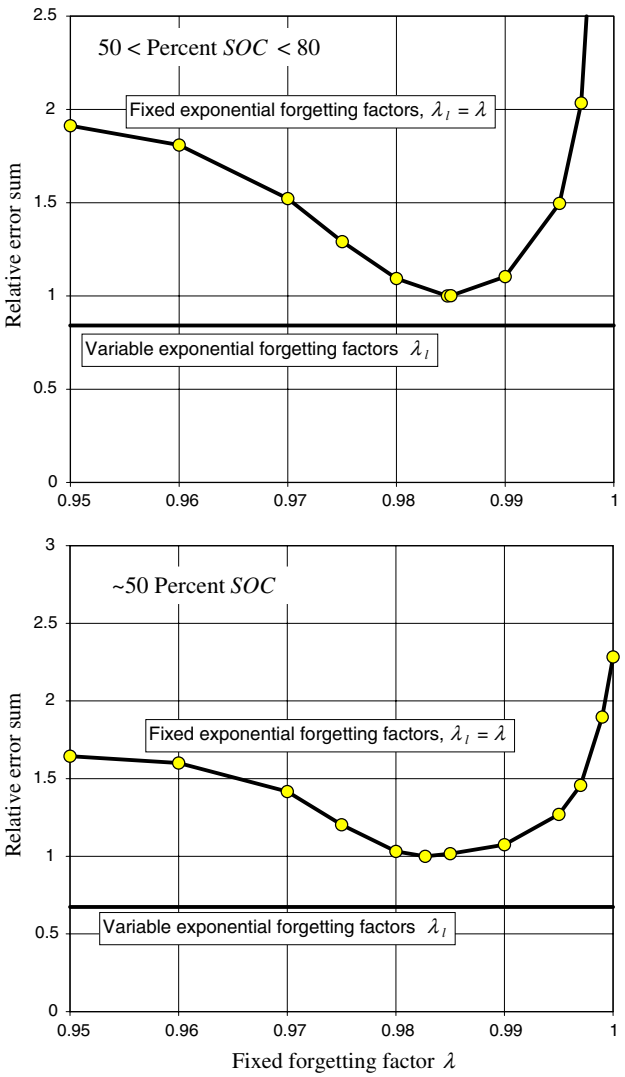

Fig. 5 Relative error sum for the optimization of forgetting factors. The upper plot corresponds to the analyses of Fig. 3, and the lower plot to those of Fig. 4. The error is increased by 18% (top) and 53% (bottom) in going to a fixed forgetting factor relative to variable forgetting factors. The variable forgetting factors indicated in the lower plot above are shown in the inset table of Fig. 6

time averaging over a longer duration, results from the optimization. Conversely, more rapid changes in the open-circuit potential are required for the high-power cycling regime, consistent with the discussion of Fig. 3, resulting in a smaller forgetting factor for V_o. Lithium ion and NiMH batteries are both insertion systems wherein the average concentration of the ions in the entire electrolyte phase should not change on charge and discharge. For lithium ion batteries on discharge, lithium ions are ejected from the carbon anode and inserted into the metal oxide cathode, and there is no net change in the number of ions within the electrolyte phase. The same conclusion holds for charge, wherein lithium ions are discharged from the metal oxide cathode and inserted into the carbon anode. While local concentration gradients will influence the cell potential [24, 25, 29], to a first approximation we might expect the high-frequency resistance R to be rather constant over a drive profile, consistent with the secondary current distribution for the cell [26–28] and a constant number of charge carriers in the electrolyte phase. The same arguments hold for protons (versus lithium ions) in NiMH batteries. The fact that the algorithm yields a stable value for R is also important in the context of SOH, as it is likely that the definition

$$SOH \equiv R_{\text{nominal}}(T, SOC)/R(T, SOC) \tag{15}$$

will provide a means to rationalize the term state of health. In this relation, the nominal resistance for a (new and healthy) battery is R_{nominal}, which can be a tabulated quantity within an embedded controller so as to be a function of temperature and SOC. As will be seen below, the high-frequency resistance R plays a central role in determining the power capability; hence the defined SOH is a meaningful quantity, as the power capability of the battery is critically important to HEV operation. When electrodes degrade with time, R increases. For both lithium ion and NiMH batteries, the increase in R is often due to loss of particle-particle contact within the electrodes, the growth of ohmic layers over the particle surfaces, or the loss of solvent over time. By the definition provided in Eq. 15, we would expect new batteries to have an SOH value near unity, and the SOH would decline as the battery ages.

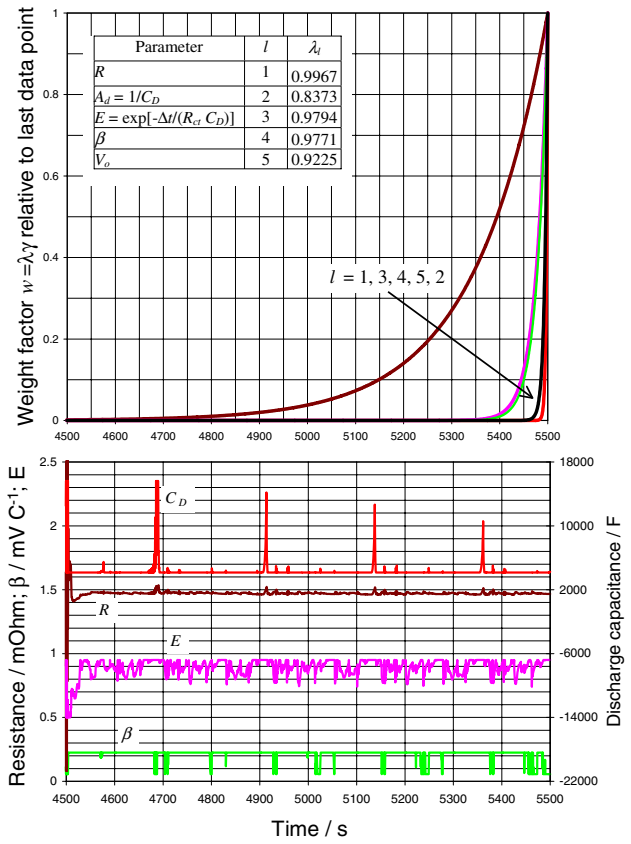

Fig. 6 Optimized (variable) forgetting factors and parameter profiles. Four of the extracted parameters are displayed in the lower plot, and the fifth (V_o) is shown in Fig. 4. The high-frequency resistance is seen to be quite stable, and a large forgetting factor, reflecting time average over a longer duration, results from the optimization. Conversely, more rapid changes in the open-circuit potential are required for the high-power cycling regime, resulting in a smaller optimized forgetting factor for V_o

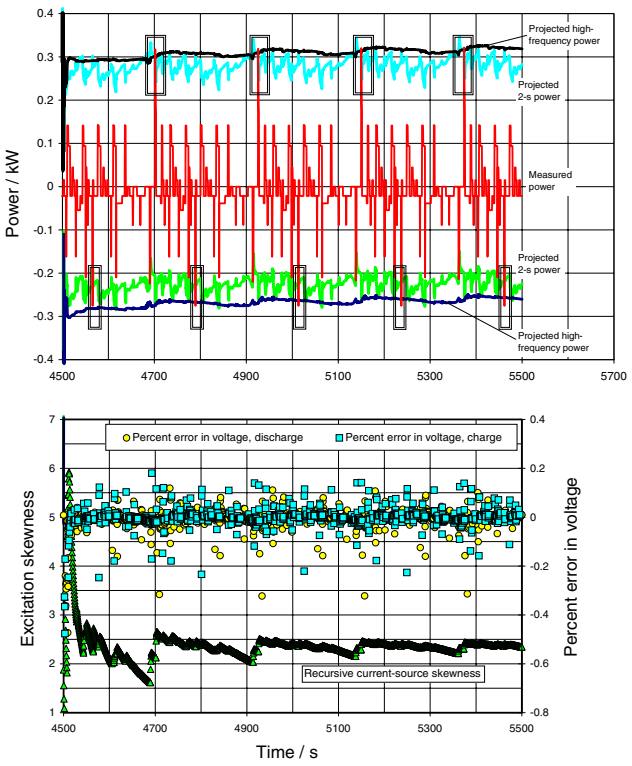

Fig. 7 Power, current-excitation skewness (Eq. 32), and percent instantaneous error in voltage model, $100[V^{\text{model}}(t) - V^{\text{measured}}(t)]/V^{\text{measure}}(t)$. The current source for these data is shown in Fig. 4. The cell power is the known (recorded) excitation source, and all other quantities plotted have been calculated using the regressed parameters values

(A short-circuit within a cell would lead to an abnormally high value of SOH, significantly greater than unity, and would imply failure of the system).

The remainder of our discussion is concerned with power projections provided by the algorithm. Eqns. 28 through 30 provide the necessary relations. Plots of the power projections provided by the algorithm along with the actual measured power are provided in Fig. 7 and 8. The skewness of the current source, depicted in the lower plot of Fig. 7, is based on the relation [30]

$$Skewness = \left| \frac{1}{N\sigma^3} \sum_{j=1}^{j=N} (x_j - \bar{x})^3 \right|, \tag{16}$$

where $\bar{x}$ is the average of the x-values and σ^2 is the variance. In this formula, x refers to the current excitation source. Large skewness in data can occur when the excitation source is substantially constant for a prolonged duration and then abruptly transitions to a new value of very different magnitude. The last portion of the Appendix shows how this formula is made fully recursive without approximation. The power, current-excitation skewness (Eq. 32), and percent error in voltage corresponding to the data of Fig. 4 are depicted in Fig. 7. We see that the local maxima in skewness (at 5,157 s) correspond to larger errors in the voltage modeling (the maximum error magnitudes are slightly greater than 0.3%). The maximum charge and discharge power tests and projections are boxed in the upper plot. The power projections depicted correspond to the high-frequency (Eqs. 28 and 29) and 2-second power capability (Eq. 30), with the latter comprehending the capacitive behavior of the system.

An expanded view of power projections is displayed in Fig. 8. In addition to the traces shown in Fig. 7, the low-frequency discharge-power capability (Eqs. 28 and 29 with the resistance corresponding to $R + R_{ct}$) is included, and the 0.5-s power projection (large circles, $\Delta t =$ 0.5 s for the implementation of Eq. 30) is shown to accurately predict the measured power; that is, using past information and the voltage set point taken to be that which is 0.5 s into the future, the algorithm is able

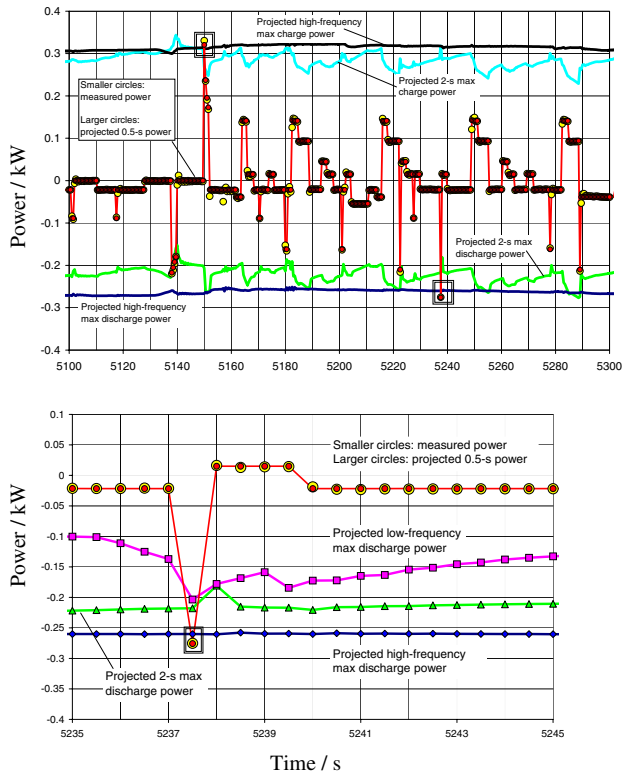

Fig. 8 Expanded view of power projections. The 0.5-s power projection (large circles, Eq. 30) is shown to accurately predict the measured power, consistent with the time per point for the measured power being 0.5 s

to predict the measured power with high accuracy. Due to charging and discharging of the capacitor circuit element (cf. Fig. 1), the 0.5-s power-projection magnitudes can exceed those of the high-frequency projection. We see that conservative battery operation is accomplished by employing the 2-s maximum power projection as the system's maximum power capability for the next 0.5 s; i.e., the risk of the voltage exceeding or dropping below the maximum or minimum voltage, respectively, is very low when the 2-s maximum power projection is employed to represent battery's maximum power capability for the next 0.5 s. The maximum error in the 0.5-s power projection is shown in the upper plot at 5,157 s, and is addressed in the skewness analysis of Fig. 7 (lower plot).

5 Conclusions

1. The recently developed battery algorithm [5] can be extended to include forgetting factors unique to each regressed parameter, and Newton's method can be employed to determine the optimal values of the forgetting factors.
2. A smaller forgetting factor, which provides a greater weight to more recent data, is found to be appropriate for the regressed open-circuit voltage V_o, while a larger value is desirable for the high-frequency resistance R; these findings are consistent with rapid changes in the SOC (state of charge) and thus V_o(SOC) for high-power cycling, yet relatively stable values of R for batteries employing insertion electrodes. Thus, as is commonly found in the application of model reference adaptive algorithms, the regressed parameter values reflect the underlying physics and chemistry of the system.
3. Employing a variable forgetting factor for a charge-sustaining hybrid utilizing a lithium ion battery increases the accuracy of the algorithm performance by about 50% in terms of assessing the power-projection capability, and the accuracy is also enhanced significantly with respect to determining the remaining energy in the battery (SOC) and the state of health.
4. The optimization process employed in this work provides general insight and a quantitative basis as to why a fixed forgetting factor of 0.99 has worked well in previous implementations of the multi-parameter algorithm [5].
5. The mathematical result we derive does not involve matrix inversion, and the method can be viewed as an iterative scheme; each parameter is regressed individually at every time step, and the parameter vector is then updated at the completion of a time step. Excellent results are obtained for the lithium ion battery investigated, which provides empirical support for the robustness of the algorithm.

Acknowledgements The authors recognize and thank Ramona Ying of General Motors R&D (Chemical and Environmental Sciences Laboratory) for acquiring the lithium ion battery data and helpful discussions with Damon Frisch and Brian Koch of the GM Electrical Center as well as Mutasim Salman of the Electrical Controls and Integration Laboratory at GM R&D.

Appendix

We provide a brief recapitulation of the model described in Reference [5] that is appropriate for the purposes of this work. The state of charge is taken as a weighted average (weight factor w_{SOC}) of values extracted by coulomb integration and voltage-based modeling:

$$SOC = w_{SOC}(SOC_C) + (1 - w_{SOC})(SOC_V). \quad (17)$$

For the coulomb-based state of charge, SOC_C,

$$SOC_C(t) = SOC(t-\Delta t) + \int_{t-\Delta t}^{t} \left[100\frac{\eta_I I}{Ah_{\text{nominal}}} - S_D\right]\frac{dt}{3600}. \quad (18)$$

The voltage-based state of charge, SOC_V, can be determined by inverting a voltage expression for the cell derived from the equivalent circuit depicted in Fig. 1 so as to extract the open-circuit potential,

$$V = V_{\text{oc}} + IR - A\int_{\zeta=t}^{\zeta=0} I(\zeta)\exp[-B(t-\zeta)d\zeta. \quad (19)$$

These two equations can be recast in recursive forms as

$$SOC_C(t) = SOC(t-\Delta t) + \left[\frac{100}{Ah_{\text{nominal}}}\left\{\frac{(\eta_I I)_{t-\Delta t} + (\eta_I I)_t}{2}\right\} - S_D\right]\frac{\Delta t}{3600} \quad (20)$$

and

$$V_t = (V_{oc} + IR)_t + \left(\frac{I_{t-\Delta t} + I_t}{2}\right)A_d r\Delta t + \exp(-B\Delta t)(V - V_{oc} - IR)_{t-\Delta t}. \quad (21)$$

Time is represented by t and I denotes current; discharge currents are taken as negative. The nominal capacity Ah_{nominal} corresponds to the ampere-hours of capacity the battery delivers when discharged from 100% SOC to 0% SOC at low rates of discharge. The self-discharge rate S_D and the current efficiency η_I are expected to vary with both temperature and SOC. The factor 3,600 has units of s/h, and the factor 100 is employed to keep a consistent percent basis. The parameters A and B correspond to $A = 1/C_D$ and $B = 1/(R_{ct}C_D) = 1/\tau$, where τ can be viewed as a time constant. A_d is the inverse of the capacitance on discharge, and r is the ratio of A for charge to that of discharge; i.e.,

$$r(T, SOC) = A_c/A_d = C_{D,\text{discharge}}/C_{D,\text{charge}}. \quad (22)$$

The open-circuit potential V_{oc} is a function of temperature, SOC_V, and a hysteresis function:

$$V_{oc} = V_o(T, SOC_V) + V_H. \quad (23)$$

A look-up table can be used to determine the SOC_V once the value of V_o is obtained. For the hysteresis contribution, we construct the following first-order differential equation to calculate a hysteresis voltage V_H:

$$\frac{\partial V_H}{\partial t} = \beta(\eta_I I - S_D)\left[V_{H,\max} - \text{sign}(I)V_H\right], \quad (24)$$

or

$$(V_H)_t \approx (V_H)_{t-\Delta t} + \beta\Delta t\{(\eta_I I - S_D)[V_{H,\max} - \text{sign}(I)V_H]\}_{t-\Delta t}. \quad (25)$$

For prolonged charge currents, or short but very large charge currents, the hysteresis voltage tends to about $V_{H,\max}$. The exact opposite holds for discharge currents, in which case the hysteresis voltage tends to $-V_{H,\max}$. Note also that if the current remains at zero for a long time, the hysteresis voltage tends to the charge-decreasing condition through self-discharge. The parameters in this equation (including $V_{H,\max}$) can be temperature and SOC dependent. While hysteresis plays a critical role in NiMH batteries, it is far less important in lead acid and lithium ion systems.

By combining the hysteresis and cell voltage expressions, we obtain

$$V_t = V_o + (V_H)_{t-\Delta t} + \beta\Delta t\left((\eta_I I - S_D)[V_{H,\max} - \text{sign}(I)V_H]\right)_{t-\Delta t} + I_t R + \left(\frac{I_{t-\Delta t} + I_t}{2}\right)A_d r\Delta t + E(V - V_{oc} - IR)_{t-\Delta t}, \quad (26)$$

where $E = \exp(-\Delta t/\tau)$. Equation 26 is the basis for the assignments provided in Eq. 12.

We now construct the power-projection capability. First, note that the max discharge power can be expressed as:

$$P_{\max,\text{discharge}} = IV = IV_{\min}. \quad (27)$$

That is, when the battery voltage obtains its lowest acceptable value, the max discharge power results. We shall refer to the ohmic battery power capability as

$$P_{\max,\text{discharge}} = IV_{\min} = \frac{(V_{\min} - V_{oc})}{R}V_{\min}, \quad (28)$$

consistent with $V = V_{oc} + IR$ for an ohmic battery. Similarly, the max charge power of the ohmic battery is given by

$$P_{\max,\text{charge}} = IV_{\max} = \frac{(V_{\max} - V_{oc})}{R} V_{\max}, \tag{29}$$

For the maximum ohmic resistance, obtained at long times (low frequency), R is replaced by $R + R_{ct}$, where R_{ct} is different for charge and discharge (cf. Fig. 1).

The ohmic battery does not address transient effects such as those correlated by the superposition integral. To improve the estimate, we employ Eq. 26 and calculate the maximum charge and discharge powers available for the time interval Δt:

$$\begin{aligned}
I|_t &= -\frac{(V_{oc} - V)_t + (AI_{t-\Delta t}\Delta t/2) + \exp(-B\Delta t)[V - (V_{oc} + IR)]_{t-\Delta t}}{R + (A_d r \Delta t/2)} \\
P_{\max,\text{discharge}}(\Delta t) &= IV_{\min} = \left[-\frac{(V_{oc} - V_{\min})_t + (A_d I_{t-\Delta t}\Delta t/2) + \exp(-B\Delta t)[V - (V_{oc} + IR)]_{t-\Delta t}}{R + (A_d r I_{t-\Delta t}\Delta t/2)}\right] V_{\min} \\
P_{\max,\text{charge}}(\Delta t) &= IV_{\max} = \left[-\frac{(V_{oc} - V_{\max})_t + (A_c I_{t-\Delta t}\Delta t/2) + \exp(-B\Delta t)[V - (V_{oc} + IR)]_{t-\Delta t}}{R + (A_d r I_{t-\Delta t}\Delta t/2)}\right] V_{\max}
\end{aligned} \tag{30}$$

where it is recognized that $r = 1$ on discharge. To implement these equations, the respective powers are calculated immediately after the algorithm has been employed to finish the *SOC* determination at time t. In this case, quantities calculated or measured at time t are then stored in the variables listed in the respective power expressions at time t–Δt. Then one must state the duration corresponding to the desired estimate for power. For example, if we want to know the power estimates 3 s from ''now'', then the measured and extracted values are placed in the t–Δt quantities, Δt is set to 3 s, and the right sides of the above equations yield the desired power estimates.

The final topic of this Appendix is the skewness test of the current source. Following the procedure described in References [4] and [5], we restrict the skewness test to the actual current values $I(t)$ and do not incorporate the charge-discharge weighting. The subscript s is added to indicate quantities associated with the skewness calculation:

$$\begin{aligned}
s_{w,s}|_N &= \sum_{j=1}^{N} \lambda^{N-j} = 1 + \lambda \sum_{j=1}^{N-1} \lambda^{N-1-j} = 1 + \lambda\left(s_{w,s}|_{N-1}\right) \\
s_{I,s}|_N &= \frac{1}{\sum_{j=1}^{N} \lambda^{N-j}} \sum_{j=1}^{N} \lambda^{N-j} I_j = \frac{I_N + \lambda\left(s_{I,s}|_{N-1}\right)\left(s_{w,s}|_{N-1}\right)}{\left(s_{w,s}|_N\right)} \\
s_{II,s}|_N &= \frac{1}{\sum_{j=1}^{N} \lambda^{N-j}} \sum_{j=1}^{N} \lambda^{N-j} I_j^2 = \frac{I_N^2 + \lambda\left(s_{II,s}|_{N-1}\right)\left(s_{w,s}|_{N-1}\right)}{\left(s_{w,s}|_N\right)}
\end{aligned} \tag{31}$$

and

$$skewness|_N = \left|\frac{(I_N - s_{I,s}|_N)^3}{\left[s_{II,s}|_N - (s_{I,s}|_N)^2\right]^{3/2}}\right| \frac{1}{N} + (skewness|_{N-1})\left(1 - \frac{1}{N}\right). \tag{32}$$

For all of the skewness calculations employed in this work, $\lambda = 0.99$ for Eqs. 31. To start the recursive calculations for skewness, the following conditions are used.

$$\begin{aligned}
s_{w,s}|_1 &= 1 \\
s_{I,s}|_1 &= I_1 \\
s_{II,s}|_1 &= I_1^2
\end{aligned} \tag{33}$$

For the first time step, $skewness|_{t=0}$ is set to *skew_cal*(we employ a value of *skew_cal* = 10). Last, we define

$$skew\_test = \begin{cases} 0 \text{ if } skewness \geq skew\_cal, \\ 1 \text{ if } skewness < skew\_cal. \end{cases} \tag{34}$$

The adaptive parameter regression analysis is not employed if the skew test is not passed, in which case:

$$\text{if } skew\_test = 0, \text{ then} (m_t)_t = (m_t)_{t-\Delta t}. \tag{35}$$

In summary, the parameter vector **m** is not updated *skew_test* = 0; however, the approach allows one to calculate the open-circuit voltage, and SOC_V can always be calculated through the use of previously extracted parameters.

References

1. Pillar S, Perrin M, Jossen A (2001) J Power Sources 96:113
2. Verbrugge MW, Tate ED (2004) J Power Sources 126:236
3. Verbrugge MW, Liu P, Soukiazian S (2005) J Power Sources 141:369
4. Verbrugge MW, Frisch D, Koch B (2005) J Electrochem Soc 152:A333
5. Verbrugge MW, Koch BJ (2006) J Electrochem Soc 153:A187

6. Gelb A (ed) (1974) Applied optimal estimation. MIT Press, Cambridge, MA
7. Anderson BDO, Moore JB (1979) Optimal filtering. Prentice-Hall, Englewood Cliffs, NJ
8. Maybeck PS (1979) Stochastic models, estimation and control, vol. 141–1 of Mathematics in science and engineering, Academic Press
9. Widrow B, Stearn SD (1985) Adaptive signal processing. Prentice-Hall, Englewood Cliffs, NJ
10. Brogan WL (1985) Modern control theory, 2nd edn. Prentice-Hall, Englewood Cliffs NJ
11. Ljnug L, Söderström T (1986) Theory and practice of recursive identification, MIT Press
12. Bellanger MG (1987) Adaptive digital filters and signal analysis. Marcel Dekker, New York, NY
13. Åström KJ, Wittenmark B (1989) Adaptive control, Addison-Wesley
14. Kulhavý R (1996) Recursive nonlinear estimation. A geometric approach. Springer, London
15. Fortescue TR, Kershenbaum LS, Ydstie BE (1981) Automatica 17:831
16. Bittanti S, Bolzern P, Campi M, Coletti E (1988) Proceedings of the American Control Conference, IEEE, Austin, Texas, pp 1530–1531, December 1988
17. Ljung L, Gunnarsson S (1990) Automatica 26:7
18. Parkum JE, Poulsen NK, Holst J (1992) Int J Control 55:109
19. Kulhavý R (1993) Int J Control 58:905
20. Vahidi A, Druzhinina M, Stefanopoulou A, Peng H (2003) Proceedings of the American Control Conference, IEEE, Denver, Colorado, pp 4951–4956, June 2003
21. Zheng Y, Lin Z (2003) IEEE transactions on circuits and systems—II: analogue and digital signal processing 50:602
22. Berndt D (1993) Maintenance-Free Batteries. Research Studies Press, Taunton, Somerset, UK
23. Conte SD, de Boor C (1980) Elementary numerical analysis, 3rd edn. McGraw-Hill, New York, NY
24. Newman J, Tiedemann W (1975) AIChE J 21:25
25. Newman J (1991) Electrochemical systems, 2nd edn. Prentice-Hall, Englewood Cliffs, NJ
26. Verbrugge MW (1995) J Electrostatics 34:61
27. Verbrugge MW (1995) AIChE J 41:1550
28. Baker DR, Verbrugge MW (1999) J Electrochem Soc 146:2413
29. Thomas KE, Darling RM, Newman J (2002) In: van Schalkwaijk W, Scrosati B (eds) chap. 12, Advances in lithium-ion batteries. Kluwer Academic/Plenum
30. Beyer WH (ed) (1976) Standard mathematical tables, 24th edn. CRC Press, Cleveland OH